

Sustainable and imperceptible augmentation of living structures with organic bioelectronic fibres

Wenyu Wang ¹, Yifei Pan ², Yuan Shui ², Tawfique Hasan ², Iek Man Lei ², Stanley Gong Sheng Ka ², Santiago Velasco-Bosom ², Yang Cao ², Susannah B. P. McLaren ², Yuze Cao ², Fengzhu Xiong ², George Malliaras ², and yan yan shery huang ²

¹University of Cambridge

²Affiliation not available

October 31, 2023

Abstract

Functional and sensory augmentation of living structures, such as the human skin and plant epidermis, offers vast opportunities for biology-machine interface, wearable health, and environmental monitoring. However, current sensor and electronic formats could be obstructive to their hosts' inherent sensations or physiological changes. Challenges are also faced in widening the augmentation of living structures without drastically increasing the global environmental and ecological burdens. Here, we demonstrate imperceptibly augmented living systems, through in situ tethering of poly (3,4-ethylenedioxythiophene) : polystyrene sulfonate (PEDOT:PSS)-based organic bioelectronic fibres. Customising fibre tether patterns and modalities enable applications from biopotential acquisition and skin-gated organic electrochemical transistors, to augmented touch and plant interfaces. The open networks formed by the intrinsically substrate-free fibres provide a biomorphic interface, while supporting direct coupling with microelectronics and e-textiles. We further demonstrate conceptual fibre formats for on-demand device repair, upgrade, and recycle, or for enhancing electromechanical stability against touch. Our work may unfold wearable technologies that are simultaneously biologically-adaptable and sustainable.

Sustainable and imperceptible augmentation of living structures with organic bioelectronic fibres

Wenyu Wang^{1,2}, Yifei Pan^{1,2}, Yuan Shui^{1,2}, Tawfique Hasan³, Iek Man Lei⁴, Stanley Gong Sheng Ka^{1,2}, Thierry Savin¹, Santiago Velasco-Bosom¹, Yang Cao^{1,2}, Susannah B. P. McLaren^{5,6}, Yuze Cao^{1,2}, Fengzhu Xiong^{5,6}, George G. Malliaras¹, Yan Yan Shery Huang^{1,2*}

Affiliations:

¹Department of Engineering, University of Cambridge; Cambridge, CB2 1PZ, UK

²The Nanoscience Centre, University of Cambridge; Cambridge, CB3 0FF, UK

³Cambridge Graphene Centre, University of Cambridge; Cambridge, CB3 0FA, UK

⁴Department of Electromechanical Engineering, University of Macau, Macao, China

⁵Wellcome Trust/CRUK Gurdon Institute, University of Cambridge; Cambridge, CB2 1QN, UK

⁶Department of Physiology, Development and Neuroscience, University of Cambridge; Cambridge, CB2 3EL, UK

*Corresponding author. Email: yysh2@cam.ac.uk

Abstract

Functional and sensory augmentation of living structures, such as the human skin and plant epidermis, offers vast opportunities for biology-machine interface, wearable health, and environmental monitoring. However, current sensor and electronic formats could be obstructive to their hosts' inherent sensations or physiological changes. Challenges are also faced in widening the augmentation of living structures without drastically increasing the global environmental and ecological burdens. Here, we demonstrate imperceptibly augmented living systems, through in situ tethering of poly (3,4-ethylenedioxythiophene) : polystyrene sulfonate (PEDOT:PSS)-based organic bioelectronic fibres. Customising fibre tether patterns and modalities enable applications from biopotential acquisition and skin-gated organic electrochemical transistors, to augmented touch and plant interfaces. The open networks formed by the intrinsically substrate-free fibres provide a biomorphic interface, while supporting direct coupling with microelectronics and e-textiles. We further demonstrate conceptual fibre formats for on-demand device repair, upgrade, and recycle, or for enhancing electromechanical stability against touch. Our work may unfold wearable technologies that are simultaneously biologically-adaptable and sustainable.

Introduction

Merging biological systems with augmentation technologies could transform the way we interact and perceive our surroundings¹⁻⁹, further underpinning crucial data collection platforms for health management and environmental monitoring¹⁰⁻¹⁶. One major goal in functional and perceptual augmentation is to provide intimate device integration with living structures while minimally perturbing the host's intrinsic biological functions. For example, thin-film technologies^{14,16} have enabled flexible electronics that conformed onto the macroscopic shape of biological surfaces, but the associated plastic substrates (~3-10s micron thick) of these devices limit moisture/gas permeability. Electronic textiles^{6,17} harness fibre materials or fibre-shaped devices for enhanced wear-comfort and breathability, but existing electronic textile fibre sizes are usually in the range of hundreds of microns, prohibiting intimate bio-integration. More recently, advances in stretchable electronics^{4,14,18}, electronic skins^{1,10,19}, nanomembrane^{3,4,20}, and nanomesh structures^{2,10,21} have unleashed augmentation technologies that are gas-permeable^{2,3,10,20,21}, and even mechanically imperceptible to the human skin^{1,10,19}. However, these device formats have only achieved limited imperceptibility against their biological hosts' multi-faceted surface and bulk functions^{22,23}. Biological pores, sensory receptors, or topography features²² could be excessively concealed when films or components with limited openness are attached over large areas of living structures. Further, pressure exertion needed for transferring and deploying ex situ-fabricated devices could preclude their use on deformation-sensitive surfaces. Taken together, the spatiotemporal diversity of living structures²³ challenges existing fabrication techniques to augment living systems with individually optimised imperceptibility.

In addition to optimising device interface imperceptibility, another grand challenge for augmented living systems is to meet pressing demands for sustainable technology development. Lithography-based microfabrication is energy and waste intensive, due to toxic chemical uses, the need for sacrificial templates, and the effort to maintain clean-environments²⁴. The production and processing of traditional fibres and textiles also generate immense carbon and water footprints^{25,26}. Furthermore, electronic and textile wastes already impose pressing crises in the current stage of industrial development^{26,27}. Considering functionalising living structures that undergo dynamic transformations, or interact with biological analytes or chemical pollutants, regular full-scale renewal of the augmentation devices is environmentally costly.

We hypothesise that an emerging pathway for augmenting living structures with bioelectronics could harness individual micro-scaled fibres as building blocks. This could resemble how spiders build designable and sophisticated networks in situ, adapted to their environments, with minimal material consumption. Designable open network architectures with tuneable fibre number density, orientation, and modalities can be tethered onto living structures (Fig. 1a). Although 3D printing is considered an environmental-friendly fabrication route²⁸ that offers on demand fabrication^{29–32}, the resolution for state-of-the-art in situ printing is limited to hundreds of micrometres^{30,31}, which compromises device imperceptibility at the biological interfaces. On the other hand, existing approaches for fibre production, such as wet spinning³³, melting spinning³⁴, or electrospinning³⁵, are effective in producing micro/nanofibers on a large scale, but falling short in achieving sophisticated bioelectronic functions. Due to the low bending stiffness and low aerial footprint for surface adhesion of micro-scaled fibres, pre-functionalised fibre networks with open architectures are difficult to manipulate, and cannot be readily transferred and attached onto target objects³⁶. Although in situ generation of fibrous scaffolds are possible^{5,37}, these techniques inherently result in micro- and nano-meshes with random fibre overlays, lacking controls in fibrous patterns, surface contacts, and mesoscale network openness (see cross-comparison in Fig. 1b).

Here, we show that by synergistically developing an in situ solution fibre tethering technique with its solution formulations, organic bioelectronic fibres for myriad applications can be created for imperceptible augmentation of living structures. Compared to contemporary fabrication capabilities, bioelectronic fibre tethering will allow efficient creation or upgrade of the fibre interface with infinitesimal material usage and waste generation (Fig. 1c). The strategy proposed could further intertwine the service durations of disposable and re-useable components, enhancing supply-chain resilience.

Results

Integrating organic bioelectronic fibres on living structures with infinitesimal material consumptions

In this work, the bioelectronic fibres are produced from a solution phase at ambient conditions, where the solution spinnability could be characterised by the ratio of shear modulus over surface tension. Using the target periphery as a template, the fibre tethering is physically guided by the

shape and position of the target object. Aided by the dynamic physically intelligent morphing mechanism of fibre tethering, in situ construction of fibre interface over a centimetre-sized target (e.g., a person's finger) does not require digital replica. In addition, the tethering process is tolerant to target movements for an electrode-patch application (Fig. 2a). Thus, the entire fibre deposition process is contactless and mask-free.

The fibre tethering process can take place on diverse biological objects, from the width of a human hair, to ridges of a fingertip and chick embryos (Fig. 2b). The bioelectronic fibre tethering process induces little perturbation to the targets' surface structures, where the force of a single fibre tethering is estimated to be in the range of 10 μN via cantilever experiments. For example, *Mimosa pudica*, a touch sensitive plant³⁸ that closes upon gentle hand touch (force $\sim 200 \mu\text{N}$), does not respond to the fibre deposition process. The mechanical effects of fibre tethering on biocompatibility is further evaluated using fragile Day-2 chicken embryos, whose development is highly sensitive to external forces and stresses³⁹. Our results show that the Day-2 chicken embryos with fibre networks on the developing tissue display normal growth rates and morphological changes through 24 hours post fibre tethering.

The fibres are spun in a solution/ wet state, meaning that abundant residual water remains in the 'wet fibre' upon surface tethering; thus, a dominant Wenzel-like fibre-surface contact state is resulted. As shown in Fig. 2c, the bioelectronic fibre forms dominant intimate attachments even down to the micrometre-level surface topographies for macroscopically convex surfaces. Thus, depending on the contact states on different surfaces, the average feature size of a single bioelectronic fibre ranges between 1 μm and 5 μm . The spatially patterned bioelectronic fibres, along with their mechanical erasability in a wet state, offer possibilities to create in situ patterning through both 'additive' and 'subtractive' modes (as shown in Fig. 2d, and further results later).

Imperceptible on-skin electrodes with tailored formats

A fresh fibre electrode on-a-fingertip (Fig. 3a), with contact impedance comparable to reported microfabricated gold nanomeshes²¹, can be created within 3 minutes of fibre tethering (Fig. 3b under the current single nozzle setting). The high success rates and consistency in deploying the fibre electrodes indicate that the functions of the fibre patch are negligibly affected by positional drifts of the target during in situ fibre tethering. Figure. 3c shows that electrocardiogram (ECG) signals acquired by the bioelectronic fibre array are highly consistent with the ECG signals

collected by a reference gel electrode at the same time. Similarly, the fibre arrays could be configured to acquire electromyography (EMG) signals, and to monitor the steady increase of EMG signal amplitudes as representing the increased electrical activities of the skeleton muscles due to external loadings (Fig. 3d).

Repairability is a potential advantage of tethering the organic bioelectronic fibres as an exposed transient electrode. For example, as shown in Fig. 3e, the fibre electrode-skin contact impedance would increase when the exposed fibres were deliberately damaged, subsequently affecting the ECG sensing performance. New fibres could then be deposited on-demand to repair the fibre electrode without affecting existing interconnections. The biopotential acquisition interface can then be fully renewed to recover the original contact impedance level and ECG sensing performance with a fraction of material inputs compared to creating a new electrode.

Next, we show that the device and contact formats of the bioelectronic fibres-on-a-fingertip can be customised to withstand various kinds of environmental and ‘touch’ perturbations simulating daily fingertip experiences. The tethered bioelectronic fibres, even in their fully exposed states, show stable electromechanical performance under various dry wearing conditions, and environmental disturbances such as water-soaking and humid (Fig. 3f). The specific conditions tested include (1) ambient wear for at least 6 hours; (2) more than 6,000 times of mouse clicking with a mean clicking force of ~ 1.5 N; (3) around 25 meters of dry frictional wear with a plastic surface with a mean normal force up to 3 N; (4) under the simulated ‘wet’ or ‘heat’ conditions without mechanical disturbance (*i.e.*, for at least 30 minutes either immersed in water or in 90 % relative humidity) (Fig. 3f). Under these conditions, no apparent macroscopic distortion to the on-skin fibre patterns was observed, and there are insignificant performance degradations in terms of interfacial contact impedance and ECG acquisition. The conformally attached bioelectronic fibres form good fibre-to-skin adhesion and would not delaminate from unperturbed wear. It is to note that the strength, and thus the electromechanical performance of the bioelectronic fibres, are affected by the level of fibre hydration. Therefore, under wet mechanical disturbances (*i.e.*, water rinsing), the exposed bioelectronic fibres on the fingertip could be unstable. Further enhancement in the ‘wet-stability’ of the device interfaces can be designed through incorporating biocompatible and biodegradable cellulose-based materials as protective layers. As a conceptual demonstration, as shown in Fig. 3g, cellulose-based fibres can be added on top of the bioelectronic fibres, to improve the overall fibre device’s electromechanical stability. With the cellulose-based protective

layers, the tethered bioelectronic fibre array can maintain its as-deposited performance for ~ 8 meters of wet friction with a normal force of ~ 0.5 N, and at least an hour of computer typing and office work. Further, the exposed fibre contact (*e.g.*, the contact connection between the bioelectronic fibres with the copper tape on the nail) could be encapsulated by a cellulose-based film. In this case, the entire fibre device on the fingertip could withstand rinsing by running water (Fig. 3h).

Intrinsically substrate-free fibres for imperceptible augmentation

We demonstrate concepts of how customising bioelectronic fibre patterns could offer myriad possibilities for imperceptibly augmented living structures. First, as both sides of the bioelectronic fibres can remain exposed when worn on the finger, the wearer (person-i) can detect another individual (person-ii)'s ECG by contacting the wearable electrode with the other person (person-ii)'s bare finger or wrist (Fig. 4a). The dual-ECG signals acquired by the fibre electrodes contain ECG characteristics of the two people: the R peaks of person-i are pointing upwards because the person-i ECG is measured from the left to right hands; while the R peaks of person-ii are pointing downwards because it is measured from right to left hands (*i.e.*, in the reverse direction compared to person-i). It is to note that the dual-ECG signals measured from the fibre electrodes show a high correlation coefficient ($P = 0.94$) with the reconstructed composite-ECG signal measured from individual's validation gel electrodes. In the future, advanced signal processing techniques, including machine learning and blind signal separation⁴⁰, could be used for ECG signal separation and identification of other minor peaks from the dual-ECG signals. Because the fibre arrays are substrate-free, and the open fibre network minimally conceal the skin surfaces, the subtle touch sensations of the volunteers are preserved so that they can simultaneously feel the blood vessel pulsations underneath the skin. In addition, the semiconducting nature of PEDOT:PSS⁴¹ offers the opportunity for it to be configured into an organic electrochemical transistor (OECT). Bioelectronic fibres are tethered to form a breathable skin-gated OECT on the fingertip, where the area of skin acts as electrolyte between the gate and the substrate-free channel fibre arrays. The conformal contact facilitates charge exchange at the skin-fibre interface, and this enables the gating of OECT using skin as the gate-channel electrolyte (Fig. 4b). The applied channel voltage at 30 s generates a positive current in the fibre array, then the current drops abruptly as expected for PEDOT:PSS channel material operating in depletion mode (*i.e.*, positive gate voltage switching

off the device, and vice versa). The removal of the gate voltage at 90 s leads to the recovery of the current (hence the recovery of the channel conductance). Repeated gate voltage pulses result in similar current responses, showing the fibre array remains structurally intact during the switching processes.

Furthermore, complementing bioelectronic fibres with other fibres of different sensing modalities at the same anatomical site offers the opportunities to create multi-modal sensors. Humans do not possess skin ‘wetness’ receptors, and ‘wetness’ is interpreted individually through perceptions of temperature and mechanical inputs⁴². The resistance of PEDOT:PSS materials is moisture dependent⁴³. As a conceptual demonstration of augmented mist pulse perception without interfering with the host’s intrinsic perception, bioelectronic fibres and colorimetric pH-responsive fibres are both looped on the index finger of a person (Fig. 4c, see Materials and Methods for the fabrication of pH-responsive fibres). The temporal resistance of bioelectronic fibres would increase upon water mist pulses. Impingement of acidic, neutral, or alkaline mist pulses onto the finger can be distinguished by simultaneously monitoring the bioelectronic fibres’ temporal resistance and the pH-responsive fibres’ colour. Dual-modal sensing (mist detection by bioelectronic fibres, and pH by colorimetric fibres) is used here, because if mists of similar pH repeatedly impinge on the fingertip, the bioelectronic fibres will indicate the mist flows by the changes in electrical resistance, but the colorimetric fibres’ colour will remain the same. Because the fibre arrays are substrate-free and minimally conceal the skin surfaces, all volunteers were able to feel the subtle sensations generated by the mist flow impingements through the fibre arrays.

Adaptive and reconfigurable fibre sensing arrays and networks

We further demonstrate adaptive and reconfigurable sensing systems based on the bioelectronic fibres (as the sensing elements), coupled with prefabricated microelectronics or e-textile wearables. The ability to control the fibre orientations (θ) enable versatile inter-connections to be made into a device. Parallel ($\theta=0^\circ$), parallelogram ($\theta=\pm 15^\circ$), and fanning ($-30^\circ < \theta < 30^\circ$) patterns have been used for various applications in this work. The estimated patterning precisions were shown to be all above $\sim 75\%$, as indicated in Fig. 5a. The patterning precision estimations are affected by the orbital spinning process-intrinsic factors including mechanical controls, and environmental disturbances (*i.e.*, wind) during patterning; but could also be a result of mis-identification due to automatic image registration of the fibres during post data analysis. Individual

fibres' continuity and form factor thus support the connection of small electronic devices such as a micro- light emitting diode (LED) without adhesives (Fig. 5b). The low deposition forces imposed by the orbital spinning and fibre tethering mean that the micro-LED could stay still by gravity and by the friction of the leaf texture during the circuit formation. In the case of the micro-LED used, its weight is $\sim 1.4 \times 10^{-5}$ N. Thus, considering the failure force per fibre during debonding is $\sim 3.5 \times 10^{-5}$ N, as few as a single fibre is sufficient to support the weight of one micro-LED. Cyclic voltammetry through the bioelectronic fibres showed that they display ohmic resistance under up to 6V/cm applied voltage, making them compatible with other low-power bio-safe electronic components. In the subsequent demonstration, distributed bioelectronic fibres on a plant could be used to connect with the micro-LED, as a display, to form a warning system for elevated levels of ammonia exposure (Fig. 5c). Ammonia is a type of n-type dopants that interacts with PEDOT:PSS in the bioelectronic fibres to cause a de-doping of the PEDOT:PSS polymer backbone⁴⁴; hence, the micro-LED dims non-reversibly upon ammonia exposure. In comparison, the micro-LED light would only dim temporarily when encountering water mist because the effect of water on the resistance of PEDOT:PSS is reversible. The designed bioelectronic fibre pattern widens the ammonia mist capture area without compromising breathability and light transmission (*e.g.*, over 90 % transmittance as shown in Fig. 2a) for photosynthesis of the leaf surface. The fibre array, which acts as a transient interface, can be renewed independent of the re-usable LED (or other discrete electronic components). The fibre arrays, after being pulled off from the leaf, could be recycled through grinding and sonication, to produce a conducting fibre-loaded ink for 3D printing (Fig. 5d).

In the third demonstration, we show a rewritable and reconfigurable fibre array and network on a leaf of a whole plant (Fig. 5e). The fibre tethering could enable a “fabrication closed-loop” of “writing, erasing, overlaying” (Fig. 5e-i) for in situ sensing interface reconfiguration and renewal. “Writing” is an additive process which involves deploying fibres in the target area; “erasing” selectively removes fibres, where the weakened strength of bioelectronic fibres in wet regions enable them to be selectively erased off on-demand without needing organic solvents; and “overlay” (as an additive process) deploys fibres over existing structures with an arbitrary alignment. This conceptual reconfigurable sensing interface could be advantageous where if the leaf surface is damaged or obstructed, then the bioelectronic fibres could be ‘renewed’ by re-routing the fibre path onto the original electrical contact connections without further perturbing the living structure (leaf). Figure. 5e-ii shows that such mask-free direct patterning supports in situ sensing interface

repair and reconstruction on living structures with minimal disruption and infinitesimal material usage.

Finally, we demonstrate interface compatibility between the fibre tethering strategy and e-textile wearables (Fig. 5f). Here, bioelectronic fibres are tethered directly onto a glove sewn with metallic conductive yarns. Such tethering provides a dry interfacial coupling which drastically decreases the contact impedance between the metallic yarn of the glove and human skins, enabling biopotential sensing through touch. Afterwards, the bioelectronic fibres, which are coupled to the e-textile through a dry mechanical interface, could be removed from the glove by dry scratching. The collected bioelectronic fibres could also be recycled for 3D printing as shown in Fig. 5d. Thus, bioelectronic fibre tethering-enabled augmentation can be considered a sustainable bridging technology, as it offers the possibility to decouple the service durations of disposable, and multi-use, quasi-permanent components.

Outlook

Envisioning a sustainable future, recent innovations in electronics and sensors have transitioned from being solely performance-driven to encompassing ‘green ethos’ to reduce their environmental impacts^{24, 45–47}. In this work, the raw materials used to fabricate the organic bioelectronic fibres and their assembled device interfaces are entirely based on earth-abundant and biocompatible materials (*e.g.*, organic semi-conductors PEDOT:PSS, and cellulose derivatives etc), not reliant on precious metals or supply-chain sensitive sources, also mitigating any potential release of toxic or nanomaterials upon disposal and entering waste streams. Further, stepping out of contemporary manufacturing schemes, we show a material and process reduction strategy for bioelectronic fibre-tethering, from creation, to repair, reconfiguration and recycle. For instance, microfabrication process is inherently an exceedingly energy demanding and centralised process ill-suited for scalable customisation; in comparison, our fibre tethering can follow an individually-adaptive fabrications with low energy consumptions. For each device comprising bioelectronic fibres, the 0.1-0.3 mg of dry mass input required for forming fibre networks is equivalent to the estimated microfibre mass released from 1 gram of synthetic fabric after machine-washing⁴⁸. A typical machine-washing cycle of 5 kg of fabrics will generate more environmental costs, especially for water consumption and microparticle production, than producing 5,000

bioelectronic fibre arrays. In other words, depending on the application scenarios, a disposable interface made with a material reduction ethos, could be an environmentally friendly complement to a fully washable or recyclable system.

In situ fibre tethering overcomes material and format conservation associated with prefabricated interfaces. Coupled with capabilities offered by functional/ microfabricated components and e-textiles, an all-in-one wearable sensor ecosystem can be envisaged to support continuous in situ hardware upgradability and superior supply-chain resilience, while minimising environmental footprint, thanks to the infinitesimal material consumption and waste generation in each upgrade of bioelectronic fibres. It is envisaged that in ongoing work, other organic electronic materials can be incorporated in a tethered fibre format in addition to the PEDOT:PSS-based polymers demonstrated here. A wide range of fibre materials (or fibre modalities) could be mixed-and-matched for tailoring the functionality and stability of the biointerface devices for diverse real-world applications. Creating structures in situ, on-demand, with virtually zero-excess functional structure generation, like many ecologically-balanced natural systems, could be encompassed for future augmented living structures.

In summary, we present in situ tethering of organic bioelectronic fibres for augmented living structures. These bioelectronic fibres are fabricated on-demand to adapt to, but not to influence with, the transformations and perceptions of living systems. The low embodied material and energy consumptions entitle the overall process of living system augmentation to leave imperceptible ecological footprints.

References

1. Wang, S. *et al.* Skin electronics from scalable fabrication of an intrinsically stretchable transistor array. *Nature* **555**, 83–88 (2018).
2. Lee, S. *et al.* Nanomesh pressure sensor for monitoring finger manipulation without sensory interference. *Science* **370**, 966–970 (2020).
3. Yan, Z. *et al.* Highly stretchable van der Waals thin films for adaptable and breathable electronic membranes. *Science* **375**, 852–859 (2022).
4. Liu, Y., Pharr, M. & Salvatore, G. A. Lab-on-Skin: A Review of Flexible and Stretchable Electronics for Wearable Health Monitoring. *ACS Nano* **11**, 9614–9635 (2017).
5. Kim, K. K. *et al.* A substrate-less nanomesh receptor with meta-learning for rapid hand task recognition. *Nat. Electron.* (2022) doi:10.1038/s41928-022-00888-7.
6. Yan, W. *et al.* Single fibre enables acoustic fabrics via nanometre-scale vibrations. *Nature* **603**, 616–623 (2022).
7. Jung, D. *et al.* Highly conductive and elastic nanomembrane for skin electronics. *Science* **373**, 1022–1026 (2021).
8. Zhou, Y. *et al.* Giant magnetoelastic effect in soft systems for bioelectronics. *Nat. Mater.* **20**, 1670–1676 (2021).
9. Ates, H. C. *et al.* End-to-end design of wearable sensors. *Nat. Rev. Mater.* **7**, 887–907 (2022).
10. Someya, T. & Amagai, M. Toward a new generation of smart skins. *Nat. Biotechnol.* **37**, 382–388 (2019).
11. Kim, J.-H. *et al.* A conformable sensory face mask for decoding biological and environmental signals. *Nat. Electron.* **5**, 794–807 (2022).
12. Giraldo, J. P., Wu, H., Newkirk, G. M. & Kruss, S. Nanobiotechnology approaches for engineering smart plant sensors. *Nat. Nanotechnol.* **14**, 541–553 (2019).
13. Kim, J., Campbell, A. S., De Ávila, B. E.-F. & Wang, J. Wearable biosensors for healthcare monitoring. *Nat. Biotechnol.* **37**, 389–406 (2019).
14. Tian, L. *et al.* Large-area MRI-compatible epidermal electronic interfaces for prosthetic control and cognitive monitoring. *Nat. Biomed. Eng.* **3**, 194–205 (2019).
15. Coatsworth, P., Gonzalez-Macia, L., Collins, A. S. P., Bozkurt, T. & Güder, F. Continuous monitoring of chemical signals in plants under stress. *Nat. Rev. Chem.* **7**, 7–25 (2022).
16. Kaltenbrunner, M. *et al.* An ultra-lightweight design for imperceptible plastic electronics. *Nature* **499**, 458–463 (2013).
17. Libanori, A., Chen, G., Zhao, X., Zhou, Y. & Chen, J. Smart textiles for personalized healthcare. *Nat. Electron.* **5**, 142–156 (2022).
18. Matsuhisa, N. *et al.* Printable elastic conductors by in situ formation of silver nanoparticles from silver flakes. *Nat. Mater.* **16**, 834–840 (2017).
19. Chortos, A., Liu, J. & Bao, Z. Pursuing prosthetic electronic skin. *Nat. Mater.* **15**, 937–950 (2016).
20. Jiang, Z. *et al.* A 1.3-micrometre-thick elastic conductor for seamless on-skin and implantable sensors. *Nat. Electron.* **5**, 784–793 (2022).
21. Miyamoto, A. *et al.* Inflammation-free, gas-permeable, lightweight, stretchable on-skin electronics with nanomeshes. *Nat. Nanotechnol.* **12**, 907–913 (2017).
22. *Functional Surfaces in Biology*. (Springer Netherlands, 2009). doi:10.1007/978-1-4020-6697-9.
23. Thompson, D. W. *On Growth and Form*. (Cambridge University Press, 1992). doi:10.1017/CBO9781107325852.
24. Franssila, S. *Introduction to Microfabrication*. (Wiley, 2010). doi:10.1002/9781119990413.
25. Niinimäki, K. *et al.* The environmental price of fast fashion. *Nat. Rev. Earth Environ.* **1**, 189–200 (2020).
26. Shi, H. H. *et al.* Sustainable electronic textiles towards scalable commercialization. *Nat. Mater.* (2023) doi:10.1038/s41563-023-01615-z.

27. Forti, V., Balde, C. P., Kuehr, R. & Bel, G. *The Global E-waste Monitor 2020: Quantities, flows and the circular economy potential*. (United Nations University/United Nations Institute for Training and Research, International Telecommunication Union, and International Solid Waste Association, 2020).
28. *The Decentralized and Networked Future of Value Creation: 3D Printing and its Implications for Society, Industry, and Sustainable Development*. (Springer International Publishing : Imprint: Springer, 2016). doi:10.1007/978-3-319-31686-4.
29. Keating, S. J., Leland, J. C., Cai, L. & Oxman, N. Toward site-specific and self-sufficient robotic fabrication on architectural scales. *Sci. Robot.* **2**, eaam8986 (2017).
30. Zhang, Y. S. *et al.* 3D extrusion bioprinting. *Nat. Rev. Methods Primer* **1**, 75 (2021).
31. Zhu, Z. *et al.* 3D Printing: 3D Printed Functional and Biological Materials on Moving Freeform Surfaces (Adv. Mater. 23/2018). *Adv. Mater.* **30**, 1870165 (2018).
32. Qin, Z., Compton, B. G., Lewis, J. A. & Buehler, M. J. Structural optimization of 3D-printed synthetic spider webs for high strength. *Nat. Commun.* **6**, 7038 (2015).
33. Ozipek, B. & Karakas, H. Wet spinning of synthetic polymer fibers. in *Advances in Filament Yarn Spinning of Textiles and Polymers* 174–186 (Elsevier, 2014). doi:10.1533/9780857099174.2.174.
34. Murase, Y. & Nagai, A. Melt spinning. in *Advanced Fiber Spinning Technology* 25–64 (Elsevier, 1994). doi:10.1533/9781845693213.25.
35. Xue, J., Wu, T., Dai, Y. & Xia, Y. Electrospinning and Electrospun Nanofibers: Methods, Materials, and Applications. *Chem. Rev.* **119**, 5298–5415 (2019).
36. Wang, W. *et al.* Inflight fiber printing toward array and 3D optoelectronic and sensing architectures. *Sci. Adv.* **6**, eaba0931 (2020).
37. Liu, G.-S. *et al.* In Situ Electrospinning Iodine-Based Fibrous Meshes for Antibacterial Wound Dressing. *Nanoscale Res. Lett.* **13**, 309 (2018).
38. Roblin, G. MIMOSA PUDICA: A MODEL FOR THE STUDY OF THE EXCITABILITY IN PLANTS. *Biol. Rev.* **54**, 135–153 (1979).
39. Kunz, D. *et al.* Downregulation of extraembryonic tension controls body axis formation in avian embryos. *Nat. Commun.* **14**, 3266 (2023).
40. Ramli, D. A., Shiong, Y. H. & Hassan, N. Blind Source Separation (BSS) of Mixed Maternal and Fetal Electrocardiogram (ECG) Signal: A comparative Study. *Procedia Comput. Sci.* **176**, 582–591 (2020).
41. Rivnay, J. *et al.* Organic electrochemical transistors. *Nat. Rev. Mater.* **3**, 17086 (2018).
42. Ackerley, R., Olausson, H., Wessberg, J. & McGlone, F. Wetness perception across body sites. *Neurosci. Lett.* **522**, 73–77 (2012).
43. Kuş, M. & Okur, S. Electrical characterization of PEDOT:PSS beyond humidity saturation. *Sens. Actuators B Chem.* **143**, 177–181 (2009).
44. Alhashmi Alamer, F. *et al.* Review on PEDOT:PSS-Based Conductive Fabric. *ACS Omega* **7**, 35371–35386 (2022).
45. Yang, Q. *et al.* Ecoresorbable and bioresorbable microelectromechanical systems. *Nat. Electron.* **5**, 526–538 (2022).
46. Kang, J., Tok, J. B.-H. & Bao, Z. Self-healing soft electronics. *Nat. Electron.* **2**, 144–150 (2019).
47. Williams, N. X., Bullard, G., Brooke, N., Therien, M. J. & Franklin, A. D. Printable and recyclable carbon electronics using crystalline nanocellulose dielectrics. *Nat. Electron.* **4**, 261–268 (2021).
48. De Falco, F., Di Pace, E., Cocca, M. & Avella, M. The contribution of washing processes of synthetic clothes to microplastic pollution. *Sci. Rep.* **9**, 6633 (2019).
49. Weiner, J. S. HUMAN PERSPIRATION. By Kuno, Yas. Springfield, Illinois: Charles C. Thomas. Blackwell Scientific Publications: Oxford. 1956. Pp. xv + 417. 72s. *Q. J. Exp. Physiol. Cogn. Med. Sci.* **42**, 327–327 (1957).
50. Schultz, C. W., Wong, J. X. H. & Yu, H.-Z. Fabrication of 3D Fingerprint Phantoms via Unconventional Polycarbonate Molding. *Sci. Rep.* **8**, 9613 (2018).
51. Millington, P. F. & Wilkinson, R. *Skin*. (Cambridge University Press, 1983).
52. *Neuroscience*. (Sinauer Associates, 2001).

Acknowledgments

We thank M.E. Welland, B. Woodington, R. Langford, S. Butler, H.T.H. Shi, S.T. Chua, S. Vignolini, and O. Windram for experimental support and advice. This work was funded by the European Research Council ERC-StG, 758865. W.W, Y.C., and Y.Y.S.H. were supported by the European Research Council ERC-StG, 758865. S.G.S.K was supported by a Sabah State Government Scholarship. S.B.P.M. and F.X. were supported by the Wellcome Trust and the Royal Society (215439/Z/19/Z). I.M.L. was supported by the Science and Technology Development Fund, Macau SAR (0119/2022/A3).

Author contributions

W.W. and Y.Y.S.H. conceived, designed experiments, and performed analysis. W.W. devised the fibre spinning set-ups and performed fibre device fabrications and characterisations, and biopotential measurements. Y.P. optimised OECT and devised the reconfigurable fibre fabrications. Y.S. performed pH fibre sensing experiments. I.M.L assisted general data analysis and S.G.S.K. assisted fibre durability and characterisations. S.V-B., Yang. C., S.B.P.M., and Y. C. assisted testing and characterisations. T.S. proposed theoretical analysis for fibre wetting. Y.Y.S.H. supervised the project, and T.H., F.X., and G.G.M. advised the project. All authors discussed results. W.W. and Y.Y.S.H. wrote the manuscript with helps from all authors.

Ethics statement

Human participant experiments were performed with the approval of the Ethics Committee of the Department of Engineering at the University of Cambridge (7/7/2021, CUEDREC) and after obtaining informed consent from volunteers. No animal protocol was required for the chicken embryonic stages studied (< 2 weeks) under the UK Animals (Scientific Procedures) Act 1986.

Competing interests

Authors declare that they have no competing interests.

Figures:

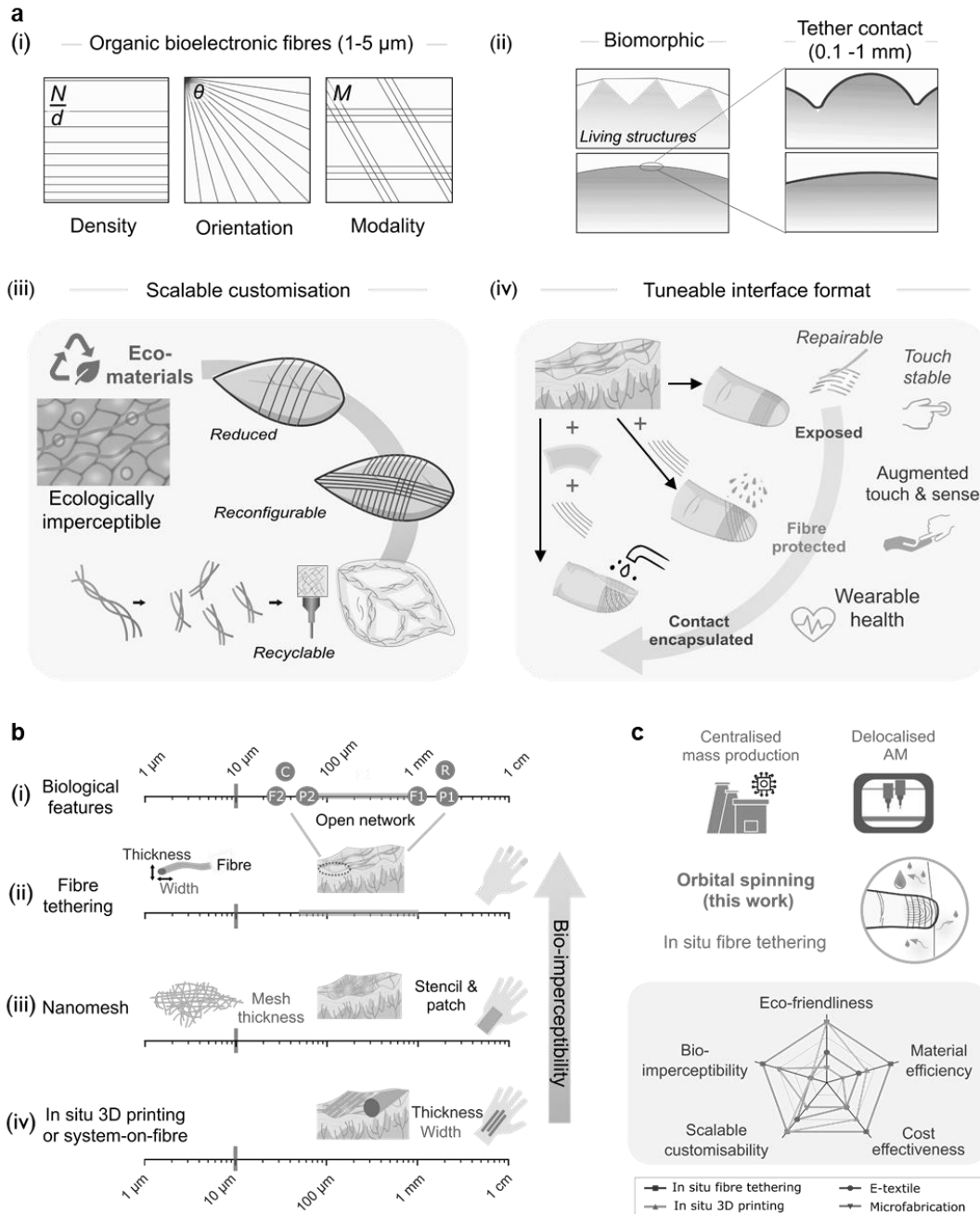


Figure 1. Imperceptibly augmented living structures with organic bioelectronic fibres. **a, (i)** fibre number density, orientation, and modalities can be customised during in situ fibre tethering; **(ii)** intimate contacts are achieved between the organic bioelectronic fibres (each $\sim 1\text{-}5\ \mu\text{m}$ wide) and different biological surfaces with micro to millimetre-scaled topographies; **(iii)** the bioelectronic fibres are fabricated on-demand with earth-abundant and biocompatible eco-materials, and individual fibres can be reconfigured and recycled. The reduction in embodied material and energy consumptions ensure the overall process of living system augmentation to be scalable and ecologically imperceptible; **(iv)** the exposed fibre electrodes (repairable and stable against touch) enable augmented touch and sensing. By customising the device format, the device

interface durability could be enhanced against various environmental disturbances for potential wearable health applications. **b**, Length scales/ feature sizes are indicated for **(i)** biological structures on the human skin of a hand, including sweat pores (density $\sim 250\text{-}500/\text{cm}^2$, symbol P1; pore size $\sim 60\text{-}80\ \mu\text{m}$, symbol P2⁴⁹), fingerprint ridges (millimetre ridge-to-ridge spacing, symbol F1; and ridge height $\sim 20\text{-}40\ \mu\text{m}$, symbol F2⁵⁰), single skin cells (sizes $\sim 30\ \mu\text{m}$, symbol C⁵¹), and receptor fields on the fingertip (\sim millimetre range, symbol R⁵²); **(ii)** bioelectronic fibre tethering for its fibre width, thickness and network opening; **(iii)** nanomesh for its mesh thickness and mesh opening. **(iv)** in situ printing or system-on-fibre (e.g. by thermal drawing) for their line (or fibre) width and thickness. A network/mesh of fibres is considered as fully skin imperceptible if it simultaneously fulfils the conditions of: (1) network/mesh opening between fibres greater than $\sim 50\ \mu\text{m}$ (c.f. the sweat gland pore size), but smaller than 1 mm (c.f. the fingertip receptor field); (2) width of individual fibres and thickness of the network/mesh smaller than $\sim 10\ \mu\text{m}$ (such that individual skin cells are mostly exposed through the open fibre network, and the fingerprint ridge features are not compromised). **c**, Orbital spinning is compared to other fabrication techniques, such as microfabrication (through centralised mass production), and 3D printing (delocalised additive manufacturing, AM) for bio-interface sensing elements. Multi-faceted key performance indicators are evaluated, where the scales of 1-4 are assigned as 4=excellent, 3= very good, 2=acceptable, and 1=needing improvements. The scores are assigned considering literature^{4-6,9,10,13,17,30,31,37}.

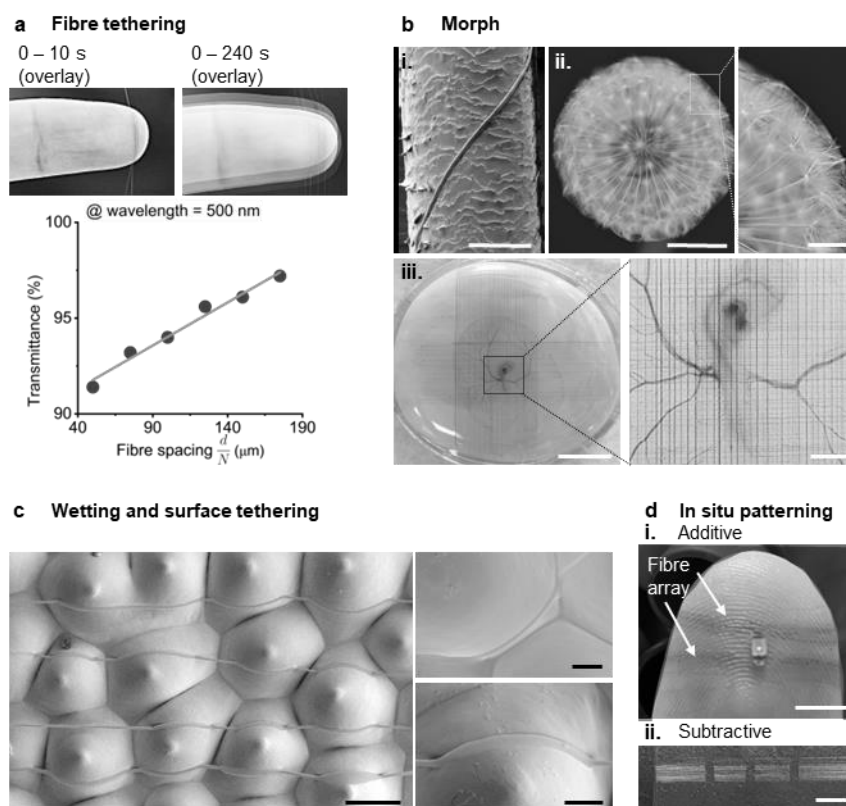


Figure 2. Organic bioelectronic fibre fabrication, morphing, and tethering on diverse biological surfaces. **a**, An example fibre deposition process is shown on a fingertip. The bioelectronic fibre array transmittance shows a seemingly linear relationship with fibre spacing $\frac{d}{N}$, with the best linear fitting of $T(\%) = 0.045\frac{d}{N} + 89$. **b**, Photos and scanning electron microscope (SEM) images showing the fibre morphing morphologies, for **(i)** A fibre (with a false colour highlight) on a human hair (scale bar = 50 μm); **(ii)** Fibres with a red colour dye conform on a dandelion seedhead, and a zoom-in view (scale bars left to right, 1 cm, 1 mm); **(iii)** fibre grids on a Day-3 chicken embryo in a petri dish, and a zoom-in view (with fibres deposited on top of the vitelline membrane covering the yolk; scale bars left to right 5 mm, 500 μm). **c**, Fibre surface tethering on an orchid flower petal (SEM images, with fibres highlighted with a false blue colour) (scale bars left to right and top to bottom, 50 μm , 10 μm , 10 μm) **d**, Concepts for fibre patterning, through **(i)** additive (fibre deposition), and **(ii)** subtractive (fibre erasing) processes. (scale bars top to bottom, 5 mm, 5 mm, 500 μm)

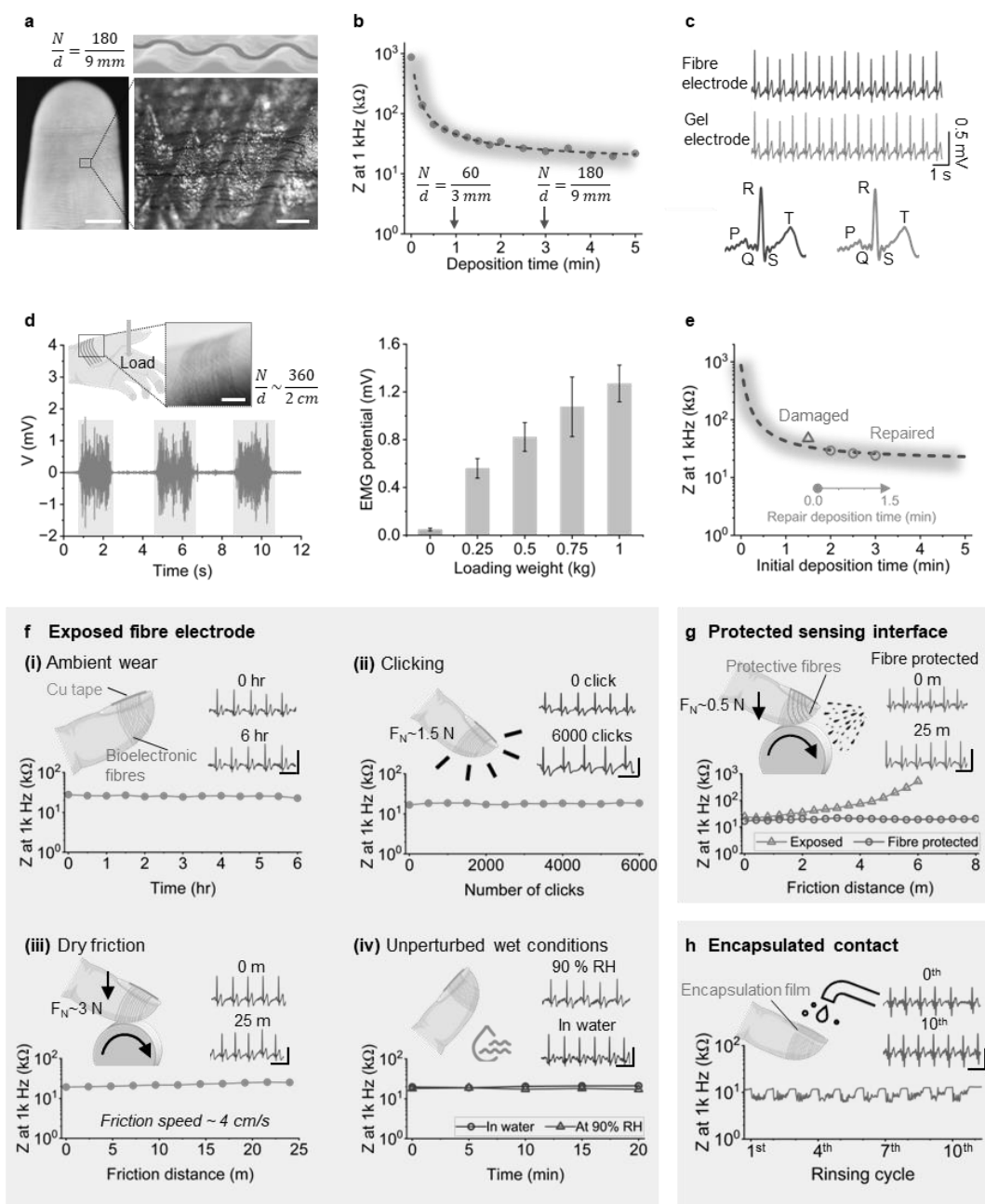


Figure 3. Imperceptible on-skin electrodes with tailored formats. **a**, Photos showing the complete fibre array on a fingertip, and the zoom-in image of the fibres follow the ridges of the fingerprints, where $\frac{N}{d}$ indicates the number of fibres across a distance (scale bars left to right, 5 mm, 500 μm). **b**, Contact impedance versus deposition time on the fingertip. **c**, Comparison of ECG signals acquired by fibre and gel electrodes at the same time (signal correlation $P=0.99$). **d**, An array of fibres deposited on the thumb muscle region to measure the EMG signal, with the variations of the EMG amplitude versus the weight of loading (scale bar, 1 cm). **e**, Facile reparability of the exposed fibre arrays. The triangular symbol indicates the impedance of the fibre arrays after being deliberately damaged by abrasion, and then new fibres are deposited on-demand to repair as indicated by the circular symbols. **f**, The stability of exposed fibre electrode (exposed bioelectronic fibres on skin) under the conditions of (i) ambient wearing; (ii) mouse clicking; (iii) dry friction wear with a plastic surface (at a surface speed of 4 cm/s); (iv) simulated ‘wet’

conditions without mechanical disturbance. **g**, Wet friction (at a surface speed of 4 cm/s) of exposed and cellulose-based fibre protected sensing interface. **h**, Rinsing under running water (the sensing interface is protected with cellulose-based fibres and the fibre contact is encapsulated with a cellulose-based film). (ECG scales for **f-g**, horizontal time scale = 1 s, vertical voltage scale = 0.5 mV). (Typical results from N=5 volunteers, with n>3 independent experiments performed on each volunteer).

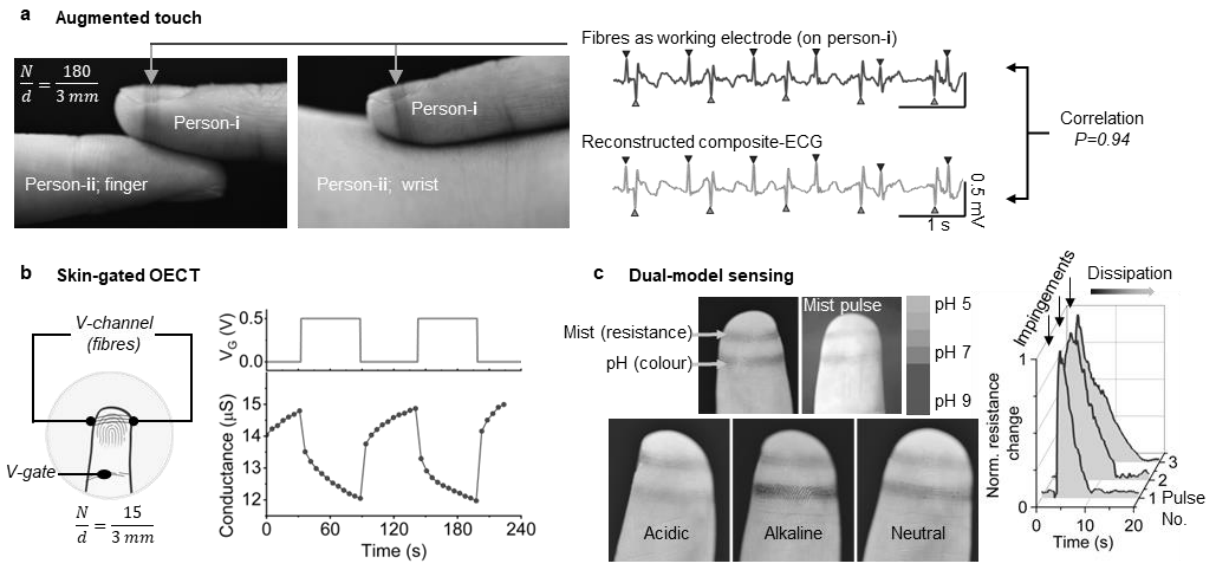


Figure 4. Imperceptible augmentation. **a**, Augmented touch perception via dual-ECG sensing with person-i wearing bioelectronic fibre arrays, and person-ii without. The dual-ECG signal acquired through the fibre array is compared with the reconstructed composite-ECG signal from validation gel electrodes. The red ▼ and green ▲ symbols indicate the R peaks of person-i and person-ii respectively. **b**, A breathable skin-gated OEET on a fingertip; the OEET displays a response time in the 60 s range. **c**, Dual-modal sensing for augmented perception of mist pulses with acidic, alkaline, and neutral compositions distinguished through colorimetric and electrical readouts (normalised resistance change is calculated as $\frac{R^* - R_0}{R_0}$, where R^* is the peak resistance, and R_0 is the initial resistance; the initial resistances of the fibre arrays are in the range of 10 k Ω). (Typical results from N=5 volunteers, with n>3 independent experiments performed on each volunteer).

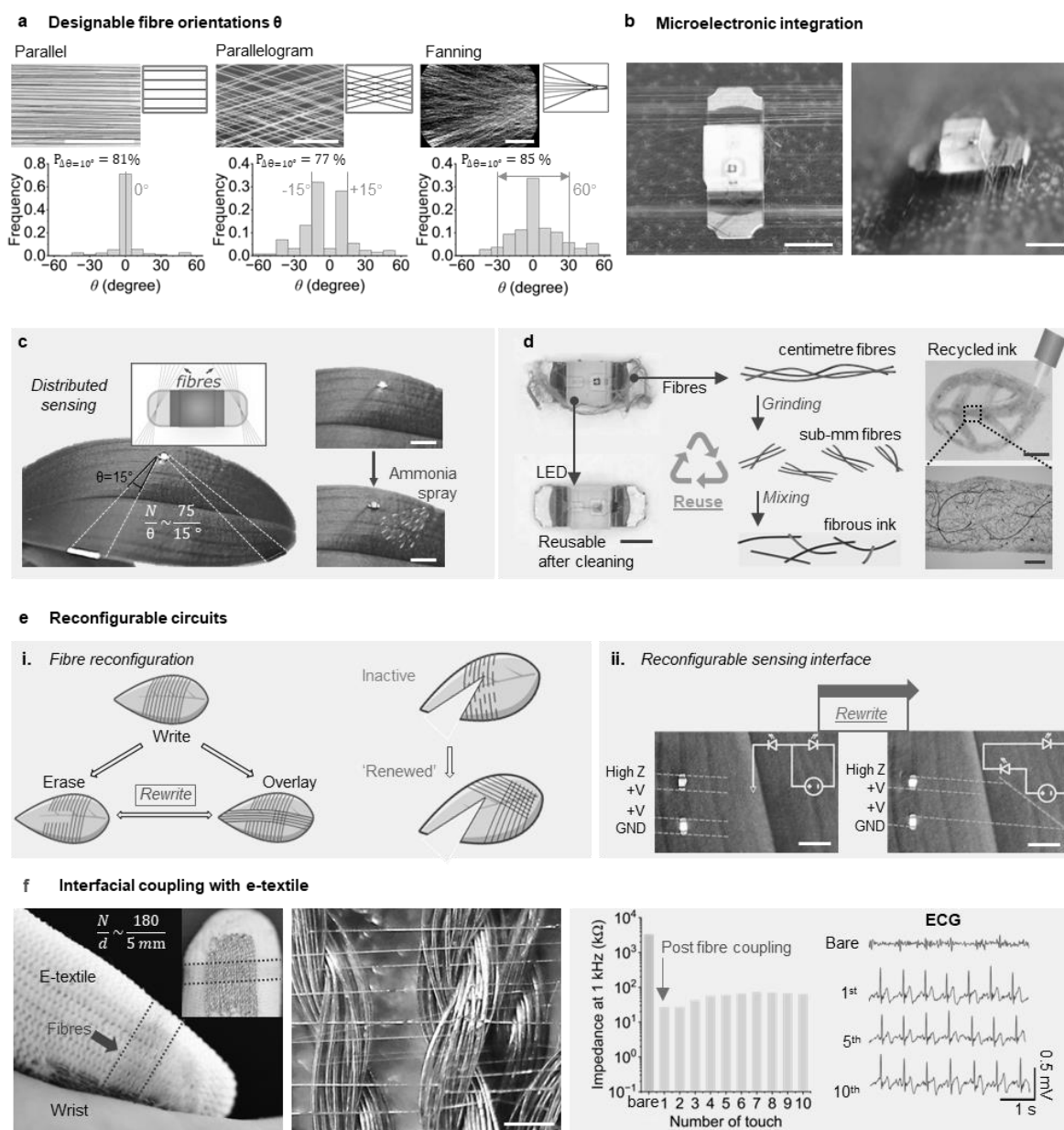


Figure 5. Adaptable, versatile, and reconfigurable fibre coupling. **a**, Fibre tethering with designable fibre orientations (θ) is demonstrated by statistical analysis of fibre orientations θ with different fibre patterns, and the patterning accuracies ($P_{\Delta\theta=10^\circ}$) is calculated by taking an 10° -offset (*i.e.*, the width of the binning in the histogram) being an acceptable criterion for misalignment (a horizontal line is used as the 0° baseline for measuring all the fibre orientation angles). **b**, Photos showing the top and profile views of fibre arrays connecting to the contacts of an LED (scale bars, 2 mm). **c**, Distributed bioelectronic fibres to connect with an LED on a plant leaf to warn environmental exposure of ammonia on the plant surfaces (where the dashed lines indicate the boundary of the fibre arrays, scale bars, 5 mm; typical results from independent experiments performed $N > 3$ plants). **d**, Concepts for re-usable and re-cyclable components, where the LED and bioelectronic fibres could be separated: the LED reused, and the fibres recycled into a feedstock to create conductive inks for 3D printing (line resistance at $\sim 1 \text{ k}\Omega/\text{mm}$ dependent on filler concentration; scale bars from left to right, and top to bottom, 1 mm, 2 mm, 500 μm). **e**, Concepts

for reconfigurable sensing interface. **i**, scheme showing a fibre fabrication and reconfiguration process, where the 'rewrite' process could help renew the fibre sensing interface; and **ii**, bioelectronic fibre arrays on the surface of a leaf which are written and rewritten to achieve a topological change in the sensing interface (for each fibre array $\frac{N}{d} \sim \frac{60}{1\text{ mm}}$; scale bars, 5 mm; typical results from independent experiments performed N>3 plants). **f**, An array of bioelectronic fibres deposited onto the finger region of an e-textile glove which reduce contact impedance by approximately 2 orders of magnitude, thus enabling biopotential monitoring (scale bar, 200 μm).